Allosteric Negative Regulation of *smt* O/P Binding of the Zinc Sensor, SmtB, by Metal Ions: A Coupled Equilibrium Analysis†

Michael L. VanZile, Xiaohua Chen, and David P. Giedroc*

Department of Biochemistry and Biophysics, Center for Advanced Biomolecular Research, Texas A&M University, College Station, Texas 77843-2128

Received March 1, 2002; Revised Manuscript Received May 30, 2002

ABSTRACT: The *Synechococcus* PCC 7942 *smt* operon is responsible for cellular resistance to excess zinc and consists of two divergently transcribed genes, *smtB* and *smtA*. SmtB is the Zn(II)-sensing metal-regulated repressor of the system and binds to a 12−2−12 imperfect inverted repeat in the *smtA* O/P region. Using fluorescence anisotropy to monitor SmtB−*smt* O/P multiple equilibria, we show that four SmtB homodimers bind to a 40 bp oligonucleotide containing a single 12−2−12 inverted repeat. The binding affinities of the first two dimers are very tight ($K_{int} = 2.9 \times 10^9$ M^{-1}) with the affinities of the third and fourth dimers lower by ≈10- and ≈30-fold, respectively. A single monomer equivalent of Zn(II), Cd(II), or Co(II) promotes disassembly of the oligomeric complex to a mixture of (P_2)·D and $(P_2)_2$·D SmtB dimer−DNA complexes with the intrinsic affinity of all SmtB homodimers for DNA greatly reduced by ≈500−2000-fold. Substitution or derivatization of cysteines which comprise the α3N metal binding site (Cys14 and Cys61) [VanZile, M. L., et al. (2002) *Biochemistry 41*, 9765−9775] has no effect on allosteric negative regulation by Zn(II); in contrast, H106Q SmtB, harboring a single zinc-liganding substitution in the α5 metal binding site, is refractory to zinc-induced disassembly of SmtB−DNA complexes. The α5 metal binding sites are therefore regulatory for Zn(II) sensing in vitro and in vivo, while the high-affinity α3N sites play some other role. This finding for SmtB is the opposite of that previously determined for *Staphylococcus aureus* pI258 CadC, a Pb(II)/Cd(II)/Bi(III) sensor [Busenlehner, L. S., et al. (2002) *J. Mol. Biol. 319*, 685−701], thus providing insight into the origin of functional metal ion selectivity in this family of metal sensor proteins.

The *smt* locus of *Synechococcus* PCC7942 consists of two divergently transcribed genes, *smtA* and *smtB*, which play roles in the cellular response to zinc and cadmium (for a review, see ref *1*) (Figure 1A). SmtB, a founding member of the SmtB/ArsR family of metalloregulatory repressors (*2*), is a homodimeric helix−turn−helix DNA binding protein (*3*) that regulates the expression of the *smtB* and *smtA* genes, the latter of which encodes a class II metallothionein that functions in the sequestration and metabolism of zinc. The solution structure of Zn(II)-complexed SmtA was recently reported (*4*). *SmtA* gene expression is repressed in the absence of heavy metals, and early studies revealed that expression was induced upon addition of Zn(II), Cd(II), and Cu(II) to the growth medium, and to a lesser extent by Co(II), Ni(II), Hg(II), Au(II), and Ag(I) (*5*). The hierarchy of metals as defined by the inducibility profile in vivo appears to correlate well with the metal affinities of SmtB in vitro, i.e., $K_{Zn} \gg K_{Co} \gg K_{Ni}$) (*6*), consistent with the idea that the relative affinities of protein−metal chelates might play some role in metal sensor selectivity in vivo (*7*).

Although the molecular details remain unclear, two studies support a simple dissociation model as the mechanism of derepression and metalloregulation by SmtB; i.e., metal binding by SmtB directly negatively regulates *smt* O/P binding (*5*, *8*). A recent report reached the opposite conclusion (*9*). The specific DNA binding affinity of a related Cd(II)/Pb(II)/Bi(III) sensor from the SmtB/ArsR family, *Staphylococcus aureus* pI258 CadC, is strongly negatively regulated by direct binding of inducing metals (*10*−*12*).

The *smt* O/P contains a pair of imperfect 12−2−12 inverted repeats designated S2/S1 and S4/S3, each of which contains a conserved core defined by the consensus sequence 5′-TGAAxx-xx-xxTTCA (Figure 1B). The S2/S1 inverted repeat is positioned at base pairs −4 to 22 relative to the start of *smtA* transcription (Figure 1). This repeat is required for regulation by SmtB and full zinc responsiveness of *smtA* expression in vivo (*8*, *13*). The S4/S3 repeat is positioned between the putative −10 and −35 sequences of the *smtA* and *smtB* promoters (Figures 1A and 2). *smt* O/P deletion studies reveal that the deletion of the S4/S3 repeat has little effect on regulation of *smtA* expression, but may be involved in autoregulation of *smtB* expression at high intracellular SmtB concentrations (*13*). Methylation protection experiments reveal that the guanosines in the S2/S1 repeat are protected from methylation at low SmtB concentrations, while those in the S4/S3 repeat require higher concentrations of SmtB, thus suggestive of weaker binding at the S4/S3 repeat (*9*). The *smt* O/P also contains a short hexanucleotide direct repeat which completely overlaps the downstream side of the 12−2−12 inverted repeat (cf. Figure 2); mutagenesis

† This work was supported by grants from the NIH (GM42569) and the Robert A. Welch Foundation (A-1295).

* To whom correspondence should be addressed. E-mail: giedroc@tamu.edu. Telephone: (979) 845-4231. Fax: (979) 862-4718.

10.1021/bi020178t CCC: $22.00
Published on Web 07/10/2002

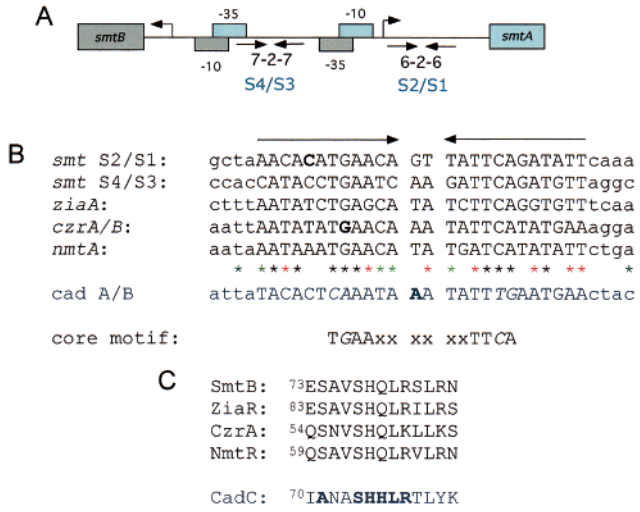

FIGURE 1: *smt* operator/promoter region. (A) Schematic representation of the *smt* operon. The *smtA* gene and its −10 and putative −35 boxes are colored blue, while the *smtB* gene and its −10 and putative −35 boxes are gray. The S4/S3 and S2/S1 sites determined by methylation interference assays (*8*) are shown to orient the Smt binding sites of interest. (B) Alignment of the DNA binding sites of SmtB with other Zn(II)/Co(II)-responsive members of the SmtB/ArsR family of metalloregulatory transcription factors (*17*). The *S. aureus* pI258 CadC binding site is shown in blue for comparison. (C) Sequence alignment of the putative recognition helices of SmtB and the other Zn(II)/Co(II)-responsive repressors.

of S2 alone, both elements of the direct repeat, or the complete S2/S1 inverted repeat all lead to high-level constitutive expression of the operator, consistent with a substantially reduced affinity for SmtB in vivo (*13*).

More recent studies carried out with the homologous Zn(II) sensor from *Synechocystis*, ZiaR (*14*), and the Zn(II)/Co(II) sensor from *S. aureus*, CzrA (ZntR) (*15*, *16*), suggest that each protein recognizes a 12−2−12 imperfect inverted repeat that conserves the central core 5′-TGAAxx-xx-xxTTCA sequence of the *smt* O/P (Figure 1B). This finding is not surprising given the high degree of sequence identity between putative recognition α-helices among SmtB, ZiaR, CzrA, and a Ni(II)/Co(II) sensor from *Mycobacterium tuberculosis*, NmtR (Figure 1C). Mobility shift assays and DNase I footprinting experiments reveal that Zn(II) or Co(II) dissociates apo-CzrA from the *czrA/B* operon, concomitant with an increased runoff transcription from the promoter in the presence of inducing metals (*15*). It has also been reported that Zn(II) in the 60−100 μM range is sufficient to dissociate all SmtB−*smt* O/P DNA complexes in vitro (*5*).

In the previous paper (*17*) as well as in previous work (*6*), we reached the surprising conclusion that the SmtB homodimer binds Zn(II) and Co(II) with a stoichiometry of two metal ions per dimer in one of *two* metal binding sites. One site, designated the α3N site, is proposed to involve coordination by Cys14 in the N-terminal arm and Cys61, just N-terminal to the α3 helix. This site appears to be populated at equilibrium in wild-type SmtB in the absence of DNA and binds Zn(II) with a K_{Zn} of $>10^{13}$ M^{-1} (*17*). The other metal binding site is found at the dimer interface and is proposed to be formed by tetrahedral coordination by Asp104 and His106 from the α5 helix in one monomer and His117′ and Cys121′ from the α5′ helix of the other subunit in the homodimer to form two symmetry-related tetrahedral sites at the dimer interface. In the absence of DNA, the α5 site appears to be filled by Zn(II) only when Cys14 and/or Cys61 is destroyed by substitution, or when all three Cys residues in SmtB are S-methylated (*17*). In the latter case, the metal coordination complex appears to be formed by Asp104, His106, His117′, and Glu120′, a sequence of Zn(II)-liganding amino acids which is invariant in all known Co(II)/Zn(II)/Ni(II) sensors in the SmtB/ArsR family, including

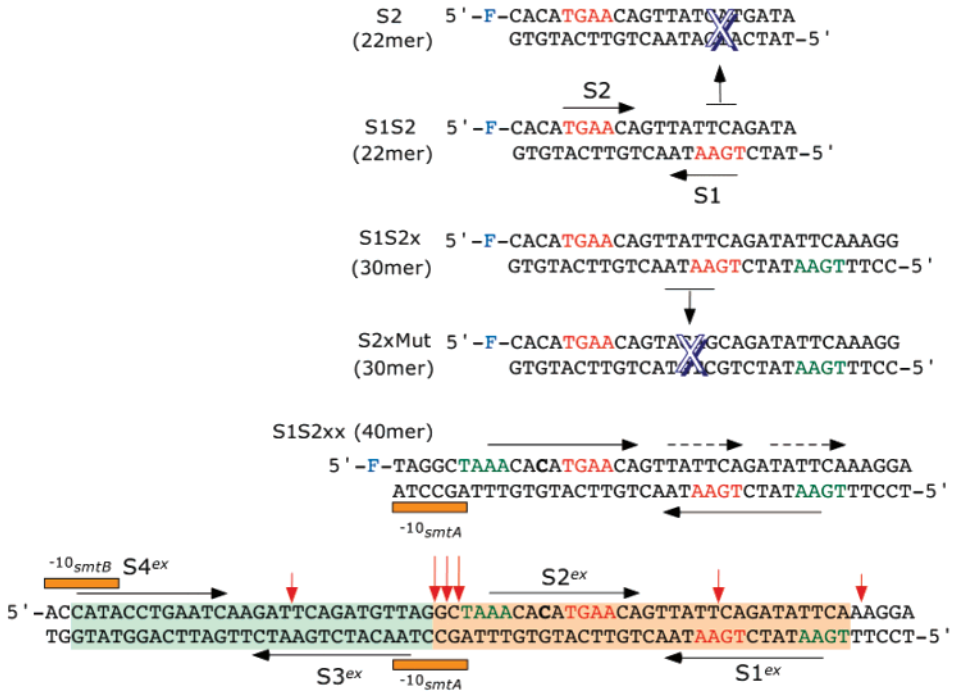

FIGURE 2: Fluorescein (F)-labeled oligonucleotides used for SmtB−DNA binding assays (see the text for details). Shown at the base of the figure is the complete sequence of the extended S1/S2 and S3/S4 sites protected from DNase I digestion by apo-SmtB in the context of an ≈100 bp *smt* O/P fragment, with sites of enhanced cleavage represented by the vertical arrows (*9*). The 32 bp S1/S2 and 31 bp S3/S4 oligonucleotides used in ref *9* are shaded in orange and green, respectively.

ZiaR, CzrA, and NmtR, as well as in some CadCs (*11*, *17*). Like the α3N site, this α5 metal binding site has a very high affinity for Zn(II) and Co(II), albeit lower than that of α3N ($K_{Zn}^{\alpha 5} \approx 10^{11}$ M^{-1}) (*17*). Strikingly, none of the three cysteine residues in SmtB are required for zinc sensing and metalloregulation in vivo (*13*). In fact, only one mutant SmtB, H105R/H106R, has been characterized which is known to abolish Zn(II) sensing in vivo (*13*); the analogous substitution (H116R) abolishes Zn(II) sensing by ZiaR as well (*14*). Since we speculate that His106 is a ligand to the Zn(II) bound in the α5 site in SmtB [similar conclusions were reached on the basis of mercuric acetate soaks of the apo-SmtB crystal structure (*3*)], these functional data are consistent with the hypothesis that the α5 site plays the primarily metalloregulatory role in vivo for Zn(II). The experiments presented here were designed to test this hypothesis.

Since the *smt* O/P is unique among the other Zn(II)/Co(II)/Ni(II) regulated operator promoters in containing an additional 12−2−12 S4/S3 repeat that appears *not* to play a primary role in the metalloregulation of *smtA* (*9*), we focused our attention here on the S2/S1 inverted repeat to obtain general insight into the mechanism of metal-induced metalloregulation of this and other SmtB/ArsR sensor proteins. Using fluorescence anisotropy to monitor SmtB−*smt* O/P binding equilibria, we establish that the stoichiometry of protein−DNA binding is two dimers per 12−2−12 inverted repeat; however, two additional dimers were found to assemble on a 40 bp oligonucleotide centered around the complete S2/S1 inverted repeat (cf. Figure 2). More importantly, in contrast to a recent report (*9*), we show that the binding of two Zn(II) ions per dimer to the α5 helical sites is necessary and sufficient to promote disassembly of the multimeric apo-SmtB complex, even when considering linkage of Zn(II) and DNA binding to the apo-SmtB monomer−dimer equilibrium (*18*).

MATERIALS AND METHODS

Chemicals. All buffers were prepared using Milli-Q deionized water. HEPES buffer salt and potassium chloride were obtained from Sigma. Ultrapure cobalt(II) chloride, cadmium(II) chloride, and zinc(II) sulfate were obtained from Johnson-Matthey.

Cell Growth and Purification of Variant SmtBs. All variants of SmtB were prepared as previously described (*17*). All variants were determined to have the expected number of reduced cysteine residues as determined by DTNB reactivity assays (*19*) and to be zinc-free [≤0.05 g of Zn(II)/mol of monomer] by atomic absorption spectroscopy on a P-E AAnalyst 700 instrument (*10*).

Preparation of Oligonucleotide Probes. Fluorescein-labeled DNA oligonucleotides (see Figure 2 for sequences) were obtained from Operon Technologies. The oligonucleotides were purified using TBE/urea gel electrophoresis followed by an 8 h elution from the gel matrix. The oligonucleotides were then desalted using a C18 column, eluted in 100% methanol, and taken to dryness in a Speed-Vac. The DNA pellets were resuspended in 200 μL of deionized water. dsDNA stocks (100 μM) were prepared in 10 mM HEPES and 0.15 M KCl (pH 7.4), heated to 95 °C, and allowed to anneal at room temperature for 3 h. Subsequent dilutions were prepared via serial 1:10 dilutions with titration buffer.

DNA Binding Anisotropy. All experiments were carried out with 40 nM dsDNA in 10 mM HEPES and 0.25 M KCl (pH 7.4) in a volume of 1.8 mL. Up to 800 μL of ∼25−35 μM protein stocks was added in known aliquots up to a total concentration of ≈8 μM. DNA binding experiments were performed in the presence and absence of 50 μM EDTA for metal-free apo-SmtB and metalated SmtB, respectively. The binding equilibria of metalated SmtBs were determined for protein titrants prepared 1:1 with metal (i.e., 1 molar equiv of metal per monomer of SmtB or 2 molar equiv per dimer). In consideration of the metal affinity for SmtB (*6*, *17*), all added metal is bound with no free metal in solution under these conditions.

The steady state anisotropy (r_{obs}) was recorded on an SLM 4800 spectrofluorometer in the ratiometric mode configured in the L-format using Glan-Thompson polarizers to select for vertically and horizontally polarized excitation (λ_{max} = 494 nm; 4 nm bandwidth) and vertically (I_{VV} and I_{VH}) and horizontally (I_{HV} and I_{HH}) polarized intensity using a Corning 515 nm cutoff filter. All I_i values were recorded following continuous excitation for 40 s and were background-corrected by subtracting I_i values measured for a solution of binding buffer, corrected for dilution, with r_{obs} calculated from the polarization (P_{obs}) using the following expressions:

$$R_{vert} = \frac{I_{VV}}{I_{VV}}$$

$$R_{horiz} = \frac{I_{HV}}{I_{HH}}$$

$$R_{corr} = \frac{R_{vert}}{R_{horiz}}$$

$$P_{obs} = \frac{R_{corr} - 1}{R_{corr} + 1}$$

$$r_{obs} = \frac{2P_{obs}}{3 - P_{obs}}$$

where R_{horiz} (the *G*-factor) was found to be 0.99 ± 0.01 in all experiments. The total fluorescence emission intensity (I_{tot}) calculated from $I_{tot} = I_{VV} + 2I_{VH}$ was found to vary in some experiments over the course of a titration, but never by more than 20% enhancement, with more typical values in the range of 5−10%. Simulations reveal that for a simple bimolecular equilibrium, r_{obs} values corrected for a 25% enhancement in total intensity as previously described (*20*) return a K_a within 10% of that obtained without considering the correction. Since this level of uncertainty is well within the standard error of K_i derived from the coupled equilibria analyzed here, the measured values of r_{obs} were therefore used directly in fitting the binding isotherms, r_{obs} versus $[\text{SmtB monomer}]_{total}$. Binding isotherms were fit using DynaFit (*21*) utilizing a model involving the sequential binding of four or (in the case of the binding of wild-type or C14S SmtB to the S1S2xx oligonucleotide) five SmtB dimers (P_2) to the DNA oligonucleotide (D) each defined by the indicated K_i, linked to the monomer−dimer equilib-

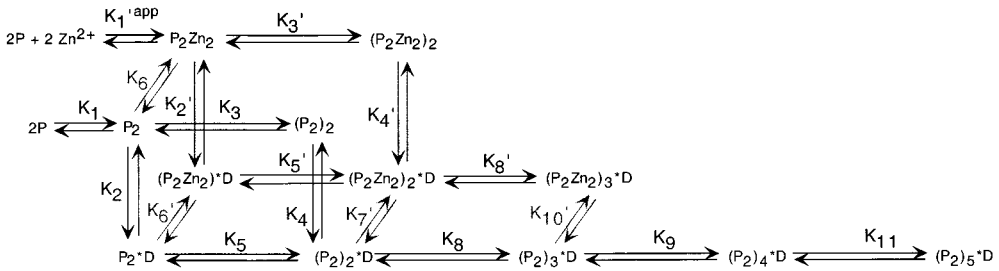

FIGURE 3: Thermodynamic linkage scheme for the coupled equilibria of SmtB self-association, Zn(II) binding, and DNA binding used to quantitatively analyze the fluorescence anisotropy-derived binding isotherms. Each K_i that is shown is for the association reaction in the presence (back of the linkage scheme) or absence (front of the linkage scheme) of two Zn(II) ions per dimer of SmtB (*17*). Higher-order oligomers of SmtB in the *absence* of DNA are not shown in the scheme since there is no evidence that SmtB oligomerizes beyond the tetramer stage. The monomer−dimer equilibrium association constants in the absence and presence of Zn(II) (K_1 and K_1', respectively) were determined to be 3.5×10^5 and 1.2×10^7 M^{-1}, respectively (*18*). The dimer−tetramer equilibrium constants (K_3 and K_3', respectively) are small under these conditions [$K_3 = K_3' = 990$ M^{-1} (*18*)].

rium (K_1) established for SmtB [cf. Figure 3 (*18*)].

$$P + P \leftrightarrow P_2;\ K_1$$

$$P_2 + D \leftrightarrow P_2{\cdot}D;\ K_2$$

$$P_2 + P_2{\cdot}D \leftrightarrow (P_2)_2{\cdot}D;\ K_5$$

$$P_2 + (P_2)_2{\cdot}D \leftrightarrow (P_2)_3{\cdot}D;\ K_8$$

$$P_2 + (P_2)_3{\cdot}D \leftrightarrow (P_2)_4{\cdot}D;\ K_9$$

$$P_2 + (P_2)_4{\cdot}D \leftrightarrow (P_2)_5{\cdot}D;\ K_{11}$$

In these fits, K_1 was fixed at the value determined by analytical equilibrium ultracentrifugation under similar solution conditions (*18*) to be 3.5×10^5 M^{-1} for apo-SmtB and 1.3×10^7 M^{-1} for Zn(II)-saturated SmtB; thus, there is strong linkage to the monomer−dimer equilibrium under these solution conditions. The characteristic anisotropies, r_i, for each $(P_2)_n{\cdot}D$ complex, i.e., $r_{P_2{\cdot}D}$, $r_{(P2)_2{\cdot}D}$, $r_{(P_2)_3{\cdot}D}$, and $r_{(P_2)_4{\cdot}D}$, were determined from stoichiometric additions of wild-type SmtB to 10 μM dsDNA. These were found to be 0.115 ± 0.001, 0.135 ± 0.002, 0.158 ± 0.002, and 0.173 ± 0.002, respectively, relative to a measured anisotropy value for the uncomplexed DNA (r_D) of 0.100, and were typically treated as fixed parameters in the resolution of K_i from all fits (cf. Tables 1 and 2). If r_D in a particular experiment was smaller or larger than 0.100, then the fixed values of r_i were linearly adjusted accordingly. The value for $r_{(P_2)_5{\cdot}D}$ was set to 0.22 in all fits when it was necessary to include it; however, the magnitude of K_{11} was found to have essentially no influence on the optimized values of K_2, K_5, K_8, or K_9 in any case due to the small value of K_{11}. These r_i values are also consistent with the r_D and $r_{P_2{\cdot}D}$ values determined independently for the binding of *S. aureus* pI258 CadC to a 34 bp fluorescein-labeled oligonucleotide (*10*). Free energies of DNA binding (ΔG_i) were determined from $\Delta G_i = -RT \ln K_i$.

RESULTS

Characterization of SmtB−DNA Binding Equilibria As Monitored by Fluorescence Anisotropy. Since it was not clear from previous studies as to what constituted the minimal site for the binding of apo-SmtB to the S2/S1 inverted repeat sequence, five different oligonucleotides (see Figure 2) were prepared and multiple SmtB−DNA binding equilibria were determined for each. For example, given the clearly palindromic nature of the S2/S1 inverted repeat and the fact that SmtB exists in solution as a dissociable homodimer, it seemed reasonable to speculate that a single SmtB dimer would bind specifically to an oligonucleotide containing a single 6−2−6 core consensus sequence of the inverted repeat (*3*). The shortest oligonucleotide, S1S2, is a 22-mer and contains the central portion of the inverted repeat but is lacking the outer two base pairs on both ends of the complete imperfect 12−2−12 repeat (cf. Figure 1B). The S2 oligonucleotide contains a 3 bp substitution which effectively destroys the core S1 5′-TGAA sequence. The 30-mer, S1S2x, is extended 8 bp on the downstream side of S1S2 and contains one half of the 12−2−12 repeat, as well as the complete direct repeat. S2xMut destroys the one half of the direct repeat as well as the inside portion of the S1 5′-TGAA sequence; this mutation was designed on the basis of a previously described mutant *smt* O/P characterized in vivo (*13*). Finally, S1S21xx contains 40 bp, encompassing the entire 12−2−12 inverted repeat flanked on both sides by 7 bp in their natural context.

Representative fluorescence anisotropy-derived binding isotherms are shown in Figure 4A under conditions of moderate salt concentration (0.25 M KCl, pH 7.4, and 25 °C) for the binding of apo-SmtB to the S1S2, S1S2x, S2xMut, and S1S2xx oligonucleotides. The solid lines through the experimental data are nonlinear least-squares fits to the sequential dimer binding model described in Materials and Methods. The binding parameters derived from these fits (K_i and r_i) and the calculated binding free energies (ΔG_i) are compiled in Table 1 and Figure 4B. The most striking observation from these experiments is that as the oligonucleotide increases in length from a 22-mer to a 30-mer to a 40-mer, the global binding isotherm shifts incrementally to the left, indicative of an increasingly higher-affinity binding in each case (Table 1) (discussed more fully below). In addition, all of the binding isotherms show little evidence of clear saturation, even in the case of the S1S2 oligonucleotide; attempts to selectively reduce or eliminate the binding of weakly bound dimers by increasing the KCl concentration, like that previously done for CadC−*cad* O/P binding equilibria (*10*), were unsuccessful. This suggests that SmtB oligomerizes or assembles on the DNA, forming complexes characterized by stoichiometries beyond that of a simple dimer binding to the S1/S2 inverted repeat. The stoichiometry

Table 1: Stepwise Equilibrium Association Constants (K_i) and Free Energy Changes (ΔG_i) for the Formation of the Individual Oligomeric $(P_2)_n$·D Species on the S1S2xx, S1S2x, S2xMut, and S1S2 Oligonucleotides in the Absence and Presence of One Monomer Equivalent of Zn(II), Co(II), or Cd(II)[a]

	S1S2xx				S1S2x[b]		S2xMut[b]		S1S2	
	P_2·D	$(P_2)_2$·D	$(P_2)_3$·D	$(P_2)_4$·D	P_2·D	$(P_2)_2$·D	P_2·D	$(P_2)_2$·D	P_2·D	$(P_2)_2$·D
apo										
K_i ($\times 10^8$ M^{-1})	29 ± 4	29 ± 4	3.4 ± 0.4	0.084 ± 0.007	1.3 ± 0.1	0.030 ± 0.004	0.11 ± 0.1	0.009 ± 0.002	0.366 ± 0.070	0.012 ± 0.002
ΔG_i (kcal/mol)	−12.9 ± 0.1	−12.9 ± 0.1	−11.6 ± 0.1	−9.5 ± 0.1	−11.0 ± 0.1	−8.8 ± 0.1	−9.6 ± 0.1	−8.12 ± 0.11	−10.3 ± 0.1	−8.3 ± 0.1
Zn(II)										
K_i ($\times 10^8$ M^{-1})	0.044 ± 0.005 (670-fold)	0.015 ± 0.003 (2000-fold)	0.003 ± 0.001 (1100-fold)	nd[b]	0.008 ± 0.001 (170-fold)	nd	–[c]	–	0.003 ± 0.001 (120-fold)	nd
ΔG_i (kcal/mol)	−9.1 ± 0.1	−8.4 ± 0.1	−7.5 ± 0.2		−8.02 ± 0.11				−7.5 ± 0.2	
Co(II)										
K_i ($\times 10^8$ M^{-1})	0.071 ± 0.006 (410-fold)	0.017 ± 0.003 (1700-fold)	0.003 ± 0.001 (1300-fold)	nd	–	–	–	–	–	–
ΔG_i (kcal/mol)	−9.3 ± 0.1	−8.5 ± 0.1	−7.4 ± 0.1							
Cd(II)										
K_i ($\times 10^8$ M^{-1})	0.040 ± 0.012 (730-fold)	0.051 ± 0.019 (570-fold)	0.001 ± 0.0005 (3600-fold)	nd	–	–	–	–	–	–
ΔG_i (kcal/mol)	−9.0 ± 0.2	−9.2 ± 0.2	−6.8 ± 0.3							

[a] All experiments were performed with 40 nM oligonucleotide in 10 mM HEPES and 0.25 M KCl at pH 7.4 and 25 °C. Association constants (K_i) for each binding event were resolved as described in Materials and Methods as defined by the coupled equilibrium scheme outlined in Figure 3. The magnitude of reduction in K_i in the presence of Zn(II), Co(II), or Cd(II) is given in parentheses. [b] nd, K_i value for the formation of the indicated $(P_2)_n$·D complex was treated as an adjustable parameter but was $\leq 1 \times 10^5$ M^{-1}. [c] Not determined.

of binding of SmtB to S1S2 is essentially two dimers per DNA molecule, with K_{app} values for the first (K_2) and second (K_5) dimers of 3.7×10^7 and 1.2×10^6 M^{-1}, respectively (Table 1). Isothermal titration calorimetry experiments are consistent with this stoichiometry of binding to the S1S2 oligonucleotide, with significant heat evolved for the binding of the two dimers (data not shown). Although SmtB binds relatively weakly to S1S2, the binding is specific since mutation of one half of the 5′-TGAAxx-xx-xxTTCA inverted repeat in the S2 oligonucleotide lowers the affinity of apo-SmtB such that a stable complex cannot be detected under these conditions ($K_{app} < 10^5$ M^{-1}) (data not shown).

The binding of apo-SmtB to the 30 bp S1S2x oligonucleotide occurs such that the affinity of the first dimer (K_2) is increased 4-fold relative to that of S1S2 [$K_2 = (1.3 \pm 0.1) \times 10^8$ M^{-1}] as are the affinities of the second and third dimers (~3-fold) (Table 1). This suggests that significantly more contacts are formed between the apo-SmtB dimer and one half of the extended inverted repeat, relative to S1S2, consistent with the functional studies (*13*). Furthermore, if the S1 half-site is mutated in the context of S1S2x (S2xMut), essentially all of the enhanced binding affinity that is gained in going from the S1S2 to the S1S2x oligonucleotide is lost, consistent with in vivo data which suggest that the S1 half-site is functionally important (*13*) (Table 1 and Figure 4). A stoichiometry of two dimers per S1S2x oligonucleotide is consistent with previous analytical equilibrium ultracentrifugation experiments carried out with the 32-mer centered over the extended S2/S1 sites (*9*).

Finally, the highest-affinity apo-SmtB binding is observed with the longest oligonucleotide tested, S1S2xx (Figure 4 and Table 1). Here, K_2 for the loading of the first dimer is increased ~30-fold over that of S1S2x [$K_2 = (2.9 \pm 0.4) \times 10^9$ M^{-1}]; strikingly, the affinity of the second dimer (K_5) is now of the same magnitude of the first dimer, with a K_5 of $(2.9 \pm 0.4) \times 10^9$ M^{-1}, or 1000-fold larger than on S1S2x, and both indicative of nearly stoichiometric binding. Here, K_2 and K_5 are calculated from $\sqrt{K_2K_5}$ due to the inability to resolve K_2 and K_5 under these conditions (40 nM DNA). Concomitant with the increase in the affinity of the second dimer, a third dimer and fourth dimer also bind with non-negligible affinities: $K_8 = (3.4 \pm 0.4) \times 10^8$ and $K_9 = (8.5 \pm 0.7) \times 10^6$ M^{-1}, respectively. To fit the very high protein concentration range of the S1S2xx binding isotherms, it was necessary to invoke the binding of a fifth dimer; which binds with significantly lower affinity than the others (Figure 4 and Table 1).

Regulatory Metal Ions Negatively Allosterically Regulate the Binding of SmtB to the S1S2xx Oligonucleotide and Promote Disassembly of the Complex. Having determined that apo-SmtB exhibits the highest binding affinity for the S1S2xx oligonucleotide, we focused our experiments on the examination of how metals influence the DNA binding equilibria on this oligonucleotide. In Figure 5A are shown representative S1S2xx binding isotherms obtained for Zn_1, Co_1, and Cd_1 SmtB (per monomer) relative to that of apo-SmtB. The solid lines are fits to the same sequential dimer binding model, with resulting binding parameters and free energies (ΔG_i) compiled in Table 1. As can be seen, Zn(II), Co(II), and Cd(II) are equally effective in strongly reducing the equilibrium binding affinity of all three dimers for the S1S2xx DNA, with K_2 and K_5 reduced ~1000-fold in the

Table 2: Stepwise Equilibrium Association Constants (K_i) and Free Energy Changes (ΔG_i) for the Formation of the Individual Oligomeric $(P_2)_n$·D Species on the S1S2xx Oligonucleotide[a]

	apoprotein				Zn(II)		
	P_2·D	$(P_2)_2$·D	$(P_2)_3$·D	$(P_2)_4$·D	P_2·D	$(P_2)_2$·D	$(P_2)_3$·D
wild type							
K_i ($\times 10^8$ M^{-1})	29[b] ± 4	29[b] ± 4	3.4 ± 0.4	0.084 ± 0.007	0.044 ± 0.005 (670-fold)	0.015 ± 0.003 (2000-fold)	0.003 ± 0.001 (1100-fold)
ΔG_i (kcal/mol)	−12.9 ± 0.1	−12.9 ± 0.1	−11.6 ± 0.1	−9.5 ± 0.1	−9.1 ± 0.1	−8.4 ± 0.1	−7.5 ± 0.2
C14S							
K_i ($\times 10^8$ M^{-1})	37[b] ± 11	37[b] ± 11	5.1 ± 1.1	0.060 ± 0.008	0.024 ± 0.005 (1600-fold)	0.021 ± 0.005 (1800-fold)	nd[c]
ΔG_i (kcal/mol)	−13.0 ± 0.2	−13.0 ± 0.2	−11.9 ± 0.1	−9.2 ± 0.1	−8.8 ± 0.1	−8.6 ± 0.1	
C61S							
K_i ($\times 10^8$ M^{-1})	76 ± 16	4.2 ± 0.3	0.08 ± 0.01	0.003 ± 0.001	0.16 ± 0.01 (480-fold)	0.0014 ± 0.0002 (3000-fold)	0.0076 ± 0.0016 (10-fold)
ΔG_i (kcal/mol)	−13.5 ± 0.1	−11.8 ± 0.1	−9.4 ± 0.03	−7.5 ± 0.1	−9.8 ± 0.1	−7.0 ± 0.1	−8.0 ± 0.1
S-methylated							
K_i ($\times 10^8$ M^{-1})	240 ± 90	3.1 ± 0.4	0.079 ± 0.006	0.002 ± 0.001	0.0090 ± 0.0011 (26000-fold)	nd	nd
ΔG_i (kcal/mol)	−14.1 ± 0.2	−11.6 ± 0.1	−9.4 ± 0.1	−7.1 ± 0.2	−8.1 ± 0.1		

[a] All experiments were performed with 40 nM S1S2xx in 10 mM HEPES and 0.25 M KCl at pH 7.4 and 25 °C. Association constants (K_i) for each binding event were resolved as described in Materials and Methods. The magnitude of the reduction in K_i in the presence of Zn(II) is given in parentheses. [b] These K_i values were estimated from $\sqrt{K_2K_5}$ due to the inability to resolve the first and second P_2 dimer binding events. [c] nd, K_i for the formation of the indicated $(P_2)_n$·D complex was treated as an adjustable parameter but was $\leq 1 \times 10^5$ M^{-1}.

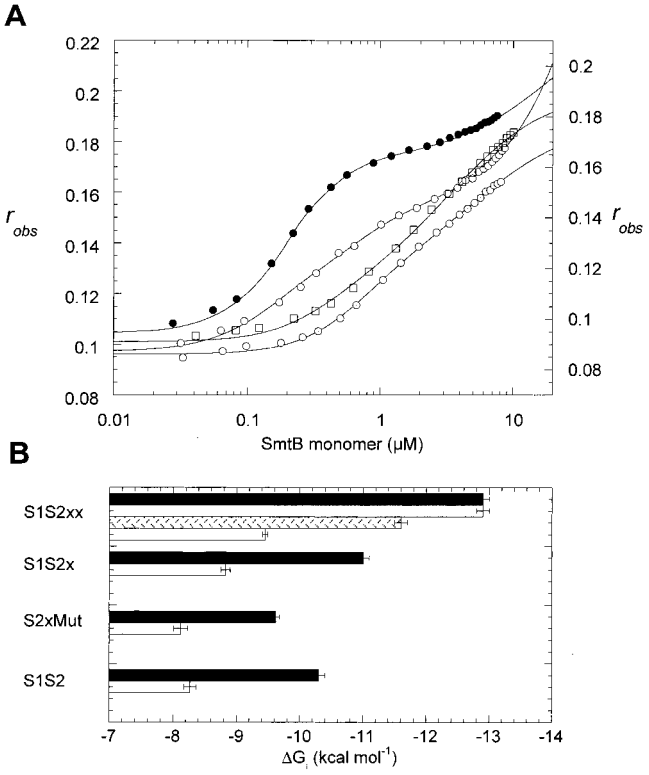

FIGURE 4: Binding isotherms for binding of wild-type SmtB with various DNA oligonucleotide probes. (A) The anisotropy, r_{obs}, is plotted vs the total wild-type SmtB monomer concentration. The data for binding of apo-SmtB to the S1S2xx (●), S1S2x (○), S2xMut (□), and S1S2 (⊙) oligonucleotides are shown. Solid lines through each of the isotherms represent nonlinear least-squares fits to the DNA binding model as described in the text with the K_i values given in Table 1. (B) Bar chart representation of the loading free energies (ΔG_i) for binding of the first (ΔG_2, solid bar), second (ΔG_5, gray bar), third (ΔG_8, stippled bar), and fourth (ΔG_9, hatched bar) dimers to each of the oligonucleotides as derived from the fitted curves in panel A. Error bars shown are those derived from fits to two or three separate experiments. Conditions: 40 nM DNA, 10 mM HEPES, 0.25 M KCl, pH 7.4, 50 μM EDTA, and 25 °C.

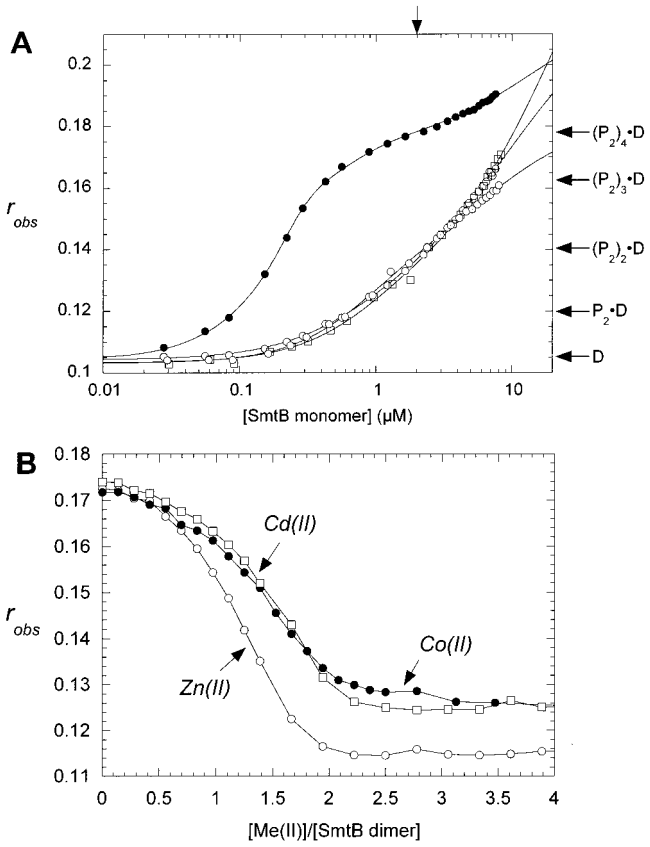

FIGURE 5: (A) Wild-type apo-SmtB binding to the S1S2xx oligonucleotide in the absence (●) and presence of stoichiometric Zn(II) (⊙), Cd(II) (□), or Co(II) (○). The anisotropy, r_{obs}, is plotted as a function of total protein concentration in monomer. The solid lines through the data represent nonlinear least-squares fits to the binding model described in the text with the K_i values compiled in Table 1. (B) Disassembly of preformed apo-SmtB complexes (2.0 μM SmtB monomer and 40 nM DNA; see the arrow in panel A) by titration of Zn(II) (○), Cd(II) (□), or Co(II) (●). Conditions: 40 nM S1S2xx DNA, 10 mM HEPES, 0.25 M KCl, pH 7.4, and 25 °C.

metalated proteins corresponding to a binding free energy that is some 4 kcal/mol less favorable (Table 1). K_8 is also substantially reduced (Table 1), and binding of a fourth dimer is not observed under these conditions.

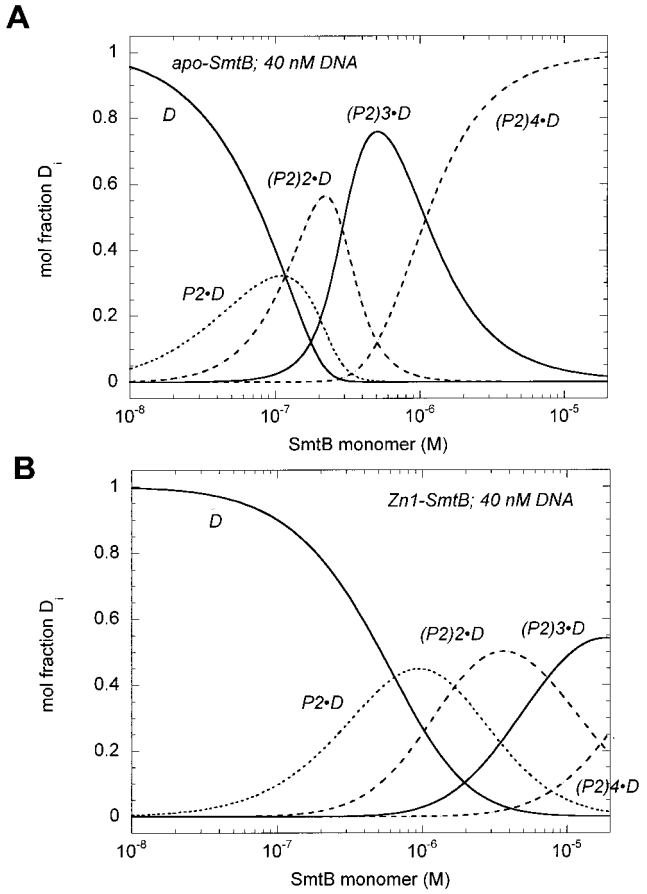

FIGURE 6: Fractional S1S2xx (*D*) species population analysis of apo-SmtB (A) and Zn_1−SmtB (B) complexes calculated for the binding isotherms of Figure 5 from the K_i values compiled in Table 1.

As shown in Figure 5B, addition of 1 molar equiv of Zn(II), Co(II), and Cd(II) per monomer to a preformed apo-SmtB−S1S2xx complex (2 μM total monomer and 40 nM DNA) is necessary and sufficient for full negative regulation of S1S2xx binding by apo-SmtB. For example, 1 molar equiv of Cd(II) and Co(II) reduces r_{obs} from the starting value of 0.174 to 0.125, both of which are exactly as expected from the direct binding isotherms (Figure 5A). Zn(II) also reduces r_{obs} to its lowest value, although in this particular experiment r_{obs} appears to be somewhat smaller than expected. In any case, note that in neither situation does r_{obs} fall to a value characteristic of free DNA, but instead falls to the value well-predicted by the direct titrations; i.e., both analyses are indeed reflective of protein and coupled metal binding at equilibrium.

Another way to visualize this is shown in Figure 6, which shows a fractional DNA species population analysis for apo-SmtB (panel A) and Zn_1-bound SmtB (panel B) throughout the course of the titrations shown in Figure 6A. At 2 μM monomer [the point at which the protein−DNA complex was dissociated by Zn(II) in Figure 5B], there is 65:35 mixture of $(P_2)_4$•D and $(P_2)_3$•D complexes, which upon addition of a single monomer equivalent of Zn(II), shifts the species population to a weighted average of 1.5 dimers/DNA, with ≈10% free DNA present. Thus, Zn(II) clearly promotes disassembly of the multimeric apo-SmtB complex. Zn(II) also negatively regulates the binding of apo-SmtB to the S1S2x and S1S2 oligonucleotides (Table 1).

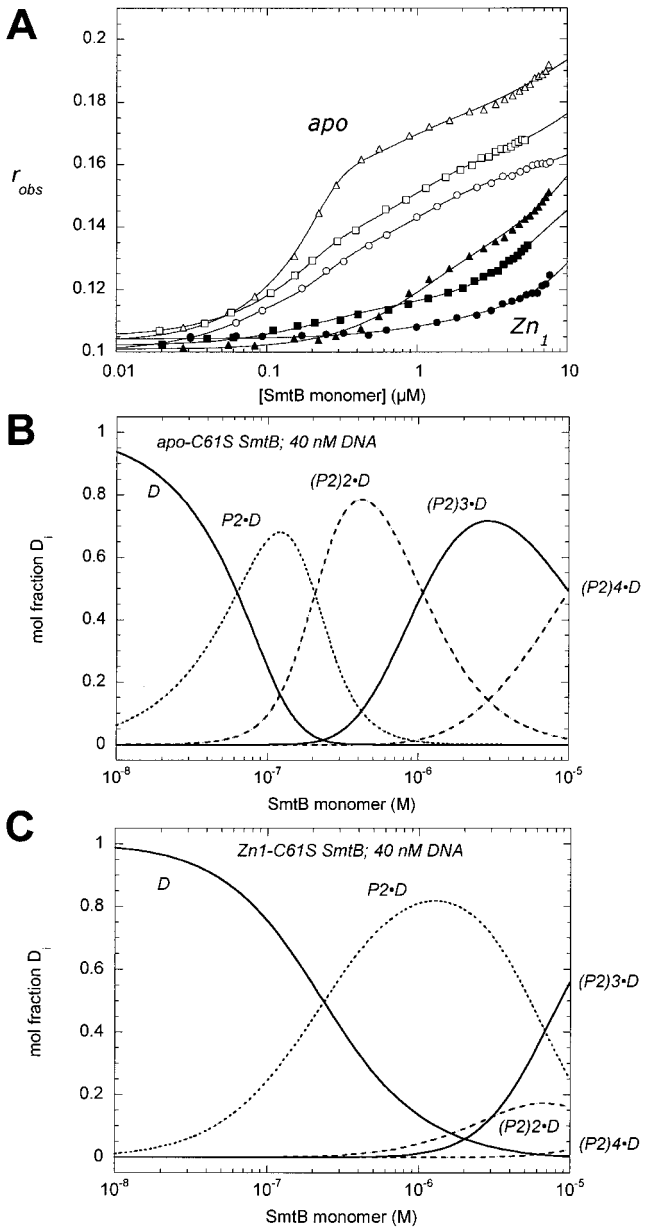

FIGURE 7: (A) DNA binding isotherms for binding of apo-C14S (△), apo-C61S (□), and apo-S-methylated (○) SmtBs to the S1S2xx oligonucleotide compared to those obtained with the Zn_1 complexes (filled symbols). The anisotropy, r_{obs}, is plotted vs the protein concentration expressed in monomer. The solid lines represent nonlinear least-squares fits to the model described in the text with the K_i values summarized in Table 2. Fractional S1S2xx (*D*) species population analysis of apo-C61S SmtB (B) vs Zn_1−C615 SmtB (C) complexes calculated for the binding isotherms of panel A from the K_i values compiled in Table 2. Conditions: 40 nM S1S2xx DNA, 10 mM HEPES, 0.25 M KCl, pH 7.4, and 25 °C.

Mutagenesis or Derivatization of the α3N Metal Binding Cysteines Has No Effect on Allosteric Regulation of smt O/P Binding by Zn(II). It was next of interest to determine the extent to which the DNA binding activity of the cysteine mutant SmtBs characterized previously (*17*) could be negatively regulated by Zn(II) binding. Figure 7A presents representative binding isotherms for C14S, C61S, and S-methylated SmtBs as apo (empty symbols) and Zn_1 (filled symbols) proteins. Just like the situation for wild-type SmtB, Zn(II) binds very tightly to each of these proteins in forming a 1:1 complex ($K_{Zn} > 10^{11}$ M^{-1}) (*17*) and is therefore unlikely

to dissociate in solution. Note that in the previous paper it was shown that C14S SmtB binds Zn(II) only in the α5 site, as do C14S/C61S, C61S, C61S/C121S, and S-methylated SmtBs (*17*). The solid lines through the data points describe nonlinear least-squares fits to the sequential dimer binding model with the parameters collated in Table 2. The most important finding from these data is that Zn(II) binding by all SmtB cysteine variants strongly negatively regulates DNA binding; thus, Zn(II) binding to the α5 site alone appears to be necessary and sufficient for negative regulation of DNA binding. For example, C14S SmtB is essentially indistinguishable from the wild-type protein, in that it is characterized by very high-affinity binding of two dimers to the DNA, with the Zn(II) form strongly inhibited. In contrast, substitution or derivatization of Cys61 has no effect on the binding of the first dimer ($K_2 \sim 5 \times 10^9$ M^{-1}) but negatively influences the binding of the second dimer by ≈8-fold ($K_5 \sim 4 \times 10^8$ M^{-1}) and strongly negatively influences the binding of the third (and fourth) dimers to the S1S2xx oligonucleotide with K_8 and K_{11} reduced by ≈220-fold. This suggests that Cys61 plays a detectable role in modulating the assembly of the multimeric apo-SmtB complex; this is borne out by the fractional species population analysis for this mutant (Figure 7B). Interestingly, C61S SmtB has been shown to be a poorer repressor in vivo under uninduced conditions (*13*). In any case, the binding affinities of all four cysteine substitution and/or derivatized forms of SmtB are strongly negatively regulated by Zn(II) in vitro (Figure 7A,C) and in vivo (*13*).

The α5 Metal Binding Site Is Required for Zn(II)-Mediated Disassembly of the Apo-SmtB−DNA Complex. Previous metal binding experiments showed that a conservative substitution of His106 for Gln (H106Q) destroyed metal [Co(II)] binding to the α5 site, while maintaining detectable binding to the peripheral α3N sites (*17*). Shown in Figure 8A are representative S1S2xx binding titrations performed with apo- and Zn_1-bound H106Q SmtB [one Zn(II) per monomer] compared to that of the wild-type protein. Although a quantitative analysis of these data is complicated by an apparent perturbation in the monomer−dimer equilibrium of apo-H106Q SmtB (data not shown), it is qualitatively apparent that H106Q SmtB is characterized by a binding profile that is similar to that of wild-type apo-SmtB. In striking contrast to the wild-type protein, H106Q SmtB preincubated with one Zn(II) per monomer maintains a high affinity of binding to the S1S2xx oligonucleotide (Figure 8A). Consistent with this, titration of the H106Q SmtB−DNA complex with Zn(II) [up to 7 equiv of Zn(II) per monomer] is incapable of disassembling the complex (Figure 8B). These data reveal that His106 is obligatory for zinc sensing by SmtB in vitro, a result fully compatible with the characterization of an H105R/H106R mutant of SmtB in vivo (*13*).

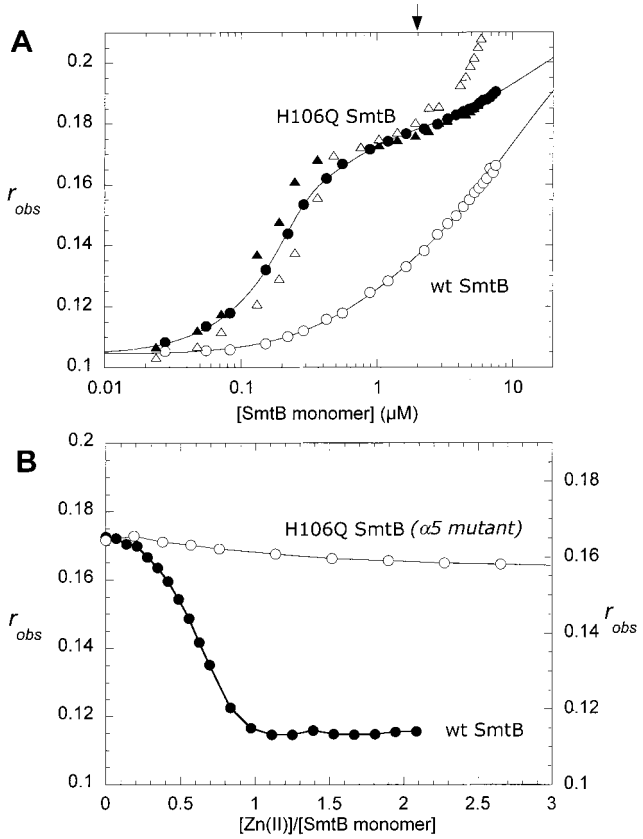

FIGURE 8: (A) Binding isotherms for binding of wild-type apo-SmtB (●) and apo-H106Q SmtB (▲) to the S1S2xx oligonucleotide vs that obtained in the presence of stoichiometric Zn(II) [H106Q (△) and wild-type SmtB (○)]. The anisotropy, r_{obs}, is plotted as a function of total protein concentration in monomer. The solid lines through the wild-type data represent nonlinear least-squares fits to the binding model described in the text with the K_i values compiled in Table 1. The binding isotherms for H106Q SmtB could not be fit since K_1 and K_1' (see Figure 3) could not be determined under these conditions. (B) Disassembly of preformed apo-wild-type (●) and H106Q (○) SmtB−S1S2xx complexes (2.0 μM SmtB monomer and 40 nM DNA; see the arrow in panel A) by titration with Zn(II). Conditions: 40 nM S1S2xx DNA, 10 mM HEPES, 0.25 M KCl, pH 7.4, and 25 °C.

DISCUSSION

The *smt* locus plays a major role in the resistance of *Synechococcus* bacterial strains to Zn(II) and Cd(II). The transcriptional repressor, SmtB, is a *trans*-acting repressor that is bound to the *smt* operator/promoter region in the absence of metals and is thought to dissociate from the DNA upon metal binding (*8*, *9*, *13*). To test this hypothesis, a series of DNA binding experiments were carried out using fluorescein-labeled DNAs (Figures 1 and 2) to determine the binding affinities of wild-type and variant SmtBs for the *smtA* operator/promoter region overlapping the S1/S2 inverted repeat in the presence and absence of inducing metals, from which a coupled equilibrium model fully consistent with our findings has been formulated (Figure 3).

Stoichiometry of SmtB Homodimer Binding to a Single 12−2−12 Inverted Repeat: Structural Implications. The fundamental stoichiometry of the binding of the SmtB homodimer to a single 12−2−12 inverted repeat is two dimers per repeat, with the affinity and calorimetric enthalpy of each dimer binding increasing significantly when the number of flanking base pairs on *both* sides of the repeat is extended to 6 or 7 bp (Table 1). This stoichiometry is compatible with that found recently for 31 and 32 bp fragments centered over the extended S4/S3 ($S4^{ex}/S3^{ex}$) and S2/S1 ($S2^{ex}/S1^{ex}$) sites, respectively (colored green and orange, respectively, in the bottom part of Figure 2) by boundary velocity sedimentation and equilibrium ultracentrifugation (*9*).

A ribbon representation of two apo-SmtB dimers and the 40 bp S1S2xx oligonucleotide are shown in Figure 9A. Two

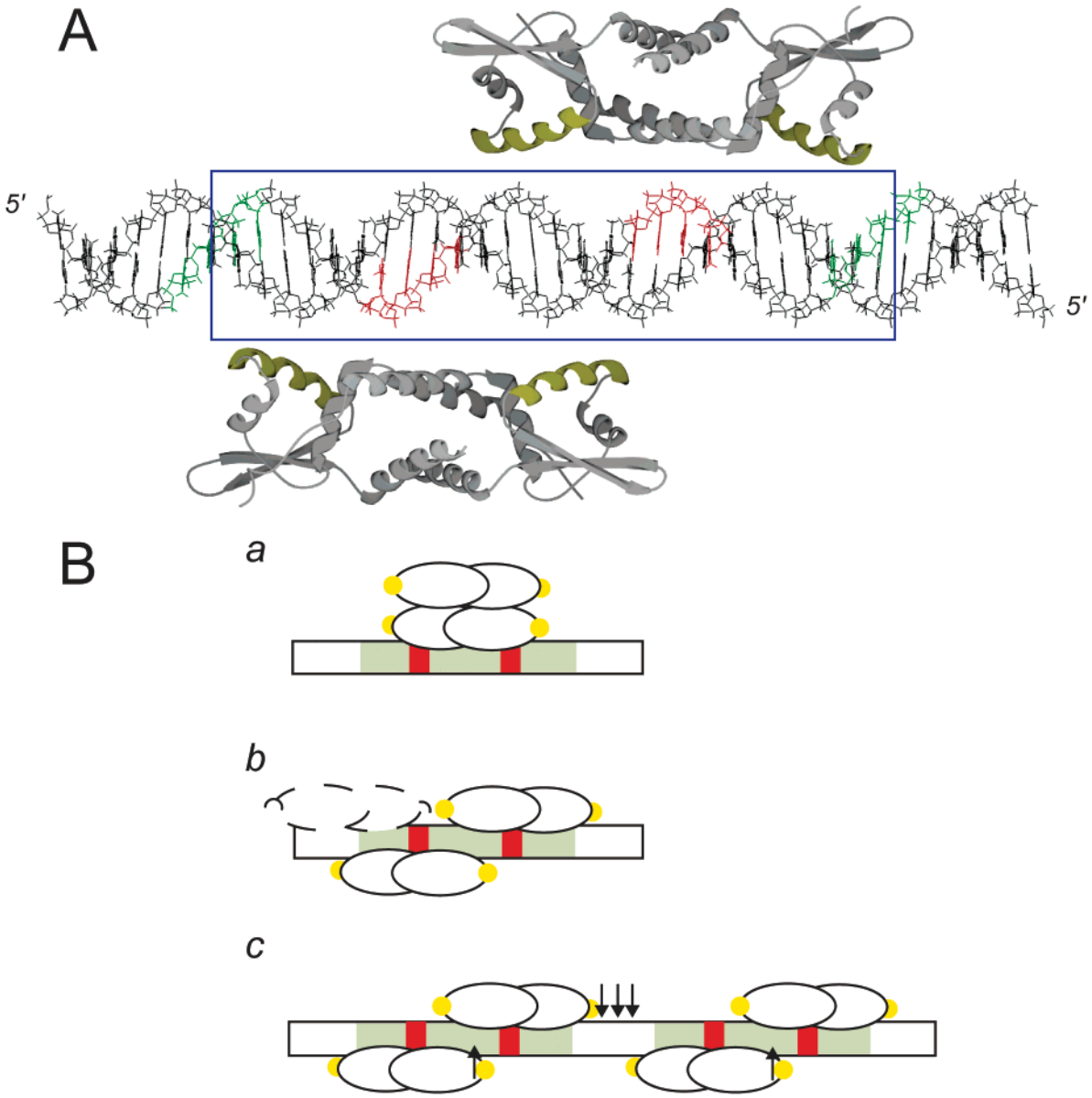

FIGURE 9: (A) Ribbon representations of two SmtB homodimers scaled to a 40 bp S1S1xx oligonucleotide drawn as straight B-form DNA. A single 12−2−12 imperfect inverted repeat is boxed, with the positions of the two 5′-TGAA repeats associated with S1 and S2 colored in red, with the two "outside" 5′-T(G/A)AA repeats colored green (cf. Figure 2). (B) Cartoon models of the dimer-of-dimers (*a*) and two-dimer-binding (*b*) models proposed to assemble on the S2S1xx oligonucleotide, with an extension of the two-dimer-binding model to a full *smt* O/P site (*c*), which might rearrange to a $(P_2)_2$·D looped complex in which two of the four bound dimers dissociate (*9*) (see the text for details). The red boxes represent the 5′-TGAA repeats within the entire imperfect 12−2−12 inverted repeat (shaded green). The yellow spheres represent the approximate position of Cys61 within each subunit of the homodimer.

possible structural models for the organization of two SmtB homodimers on this oligonucleotide are shown in Figure 9B (models *a* and *b*). In model *a*, a single dimer binds to the inverted repeat, with the second dimer binding essentially only to protein on the backside of the molecule, i.e., forming a dimer-of-dimers complex. This model is supported by the fact that SmtB homodimers have been shown to form weak tetramers in solution (*18*), although nothing is known about the structure of these tetramers. In model *b*, each of two dimers binds on opposite sides of the DNA, with each dimer nearly centered on a conserved 5′-TGAA repeat. We favor model *b* because this structure readily explains how increasing the number of flanking base pairs on *both* sides of the repeat would increase the number of intermolecular contacts, thus increasing the overall affinity (Figure 4) and altering the enthalpic signature as measured by isothermal titration calorimetry (data not shown) of the $(P_2)_2$·D complex in moving from the S1S2 to the S1S2x to the S1S2xx oligonucleotide. This is not easily explained in the dimer-of-dimers DNA complex. Such an arrangement of bound dimers is also compatible with the finding that the DNase I footprint of the homologous metal sensor pI258 CadC is offset from the center of the inverted 12−2−12 repeat (*22*) to a point nearly centered over the downstream 5′-TCAA repeat in the *cad* O/P (analogous to the 5′-TGAA repeat in the smt O/P; see Figure 1B). CadC is known only to form only a dimeric P_2·D complex under high-salt conditions (*10*, *11*), although a second dimer binds with detectable affinity under low-salt conditions (L. Busenlehner and D. Giedroc, unpublished results). In addition, a DNase I hypersensitive

site is positioned here as well (Figure 2, bottom) (*9*). This model also nicely explains how a third "bridging" dimer might bind to the upstream side of S1S2xx (i.e., toward the S3/S4 site) with relatively high affinity (Table 1).

Unfortunately, neither structural model readily explains how substitution of Cys61, exposed on the surface of the protein at the periphery of the dimer, slightly alters the free energy of loading of the second and subsequent dimers to the S1S2xx oligonucleotide (Figure 7). It seems possible, however, that substitution of Cys61 might alter in some way the SmtB-induced conformational changes that are expected to occur in S1S2xx upon loading of a single dimer (*3*), rather than directly altering protein−protein interactions in the $(P_2)_2$·D complex. Interestingly, the analogous substitution in the context of pI258 CadC is also destabilizing toward DNA complex formation (*11*).

Structural Implications for the Binding of Apo-SmtB to the Full smt O/P. Although not investigated here, structural model *b* is also compatible with recent DNase I footprinting data obtained with an ≈100 bp operator/promoter fragment encompassing the entire intergenic region between the *smtA* and *smtB* genes of the *smt* locus (*9*). If our two-dimer model were extended to a DNA fragment containing both the S1/S2 and S3/S4 sites (Figure 9B, model *c*), the two inside dimers would be separated by ≈4−6 bp which would then be positioned over a region of pronounced DNase I hypersensitive cleavage (see Figure 2, bottom) precisely halfway between the two palindromes. This complex of four dimers bound might be the "bent" structural intermediate inferred by Kar et al. (*9*) which is proposed to rearrange and form a "looped" complex at high SmtB concentrations with a stoichiometry of just two dimers per full *smt* O/P, rather than four (*9*); here, the two dimers could be bound formally as a back-to-back dimer-of-dimers (as in model *a*). Formation of such a $(P_2)_2$·D complex would appear to be more readily accommodated by dissociation of the "inside" dimers, although this is not yet known.

Zn(II) Binding Promotes Disassembly of Oligomeric Apo-SmtB−smt O/P Complexes. Kar et al. (*9*) reported that the apo-SmtB−full *smt* O/P DNA complex (assembled at 7.5 μM monomer and 40 nM DNA) is completely refractory to Zn(II)-induced dissociation, as evidenced by gel mobility shift analysis and DNase I footprinting experiments. This is in contrast to previous studies (*5*, *8*) as well as those reported here. At first glance, this result directly contradicts our findings, in that we find that 1 molar equiv of metal results in significant disassembly of the apo-SmtB−S1S2xx complex (Figures 5−7). At 2 μM total monomer, Zn(II) shifts the equilibrium from one that is characterized as a mixture of $(P_2)_3$·D and $(P_2)_4$·D complexes to one that is dominated by P_2·D and $(P_2)_2$·D complexes, but clearly not one dominated by free DNA (Figure 7). This is because despite the ≈1000-fold decrease in the intrinsic affinity of individual complexes for the DNA (Table 1), a 40-fold *increase* in the apparent dimerization constant (K_1' in Figure 3) upon Zn(II) binding to SmtB partially offsets this. However, if this experiment was carried out at 7.5 μM like that of Kar et al. (*9*) instead of at 2.0 μM, only a small shift in the species population would have resulted, i.e., from a $(P_2)_4$·D complex to a mixture of $(P_2)_2$·D and $(P_2)_3$·D complexes (Figure 6). This would have been difficult to measure in our anisotropy-based binding isotherms (cf. Figure 5A), and may have been missed in the DNase I and gel mobility shift experiments (*9*). Alternatively, only in the back-to-back dimer-of-dimer "looped" complex would the α5 metal binding sites be expected to be more protected from solvent; this might hinder their metal-induced dissociation relative to the complexes characterized here.

Zn(II)-Induced Dissociation of Oligomeric Apo-SmtB−DNA Complexes Occurs via the α5 Metal Sites and Appears To Be Functionally Important in Vivo. Mutations which have no effect on zinc sensing in vivo (C14S, C61S, and C121S) (*13*) have no effect on metal-induced DNA disassembly in vitro; in fact, complete derivatization of all three Cys residues in SmtB to mixed disulfides has essentially no effect on negative regulation of DNA binding by inducing metals (Figure 7). This effectively rules out the α3N site as a site playing an obligatory role in metal sensing, since this metal site is destroyed in these mutants (*17*). In contrast, the α5 site mutant, H106Q SmtB, is characterized by nearly wild-type affinity for DNA, but is totally insensitive to Zn(II)-promoted disassembly in vitro (Figure 8). Consistent with this, an H015R/H106R mutant has been shown to be an active repressor but has lost the ability to sense Zn(II) in vivo in *Synechococcus* (*13*).

Our findings therefore clearly reveal that the primary Zn(II)-sensing role in SmtB is carried out by the α5 site, rather than the α3N site. However, it cannot be stated that the α3N site plays no regulatory role in *smt* O/P binding. In fact, Co(II) bound to the α5 site in S-methylated SmtB readily equilibrates between the α3N and α5 sites upon reduction of the mixed disulfides, despite the very high affinity of each site for metal (*17*). Although it is not yet clear if Zn(II) is characterized by the same rapid re-equilibration, the affinity of the α3N site for Zn(II) is conservatively 1−2 orders of magnitude greater than that for the α5 site in the absence of DNA (*17*). This suggests the following model (Figure 10). After Zn(II) induces disassembly of the SmtB−cognate DNA complex, the metal bound at the α5 sensing site rapidly moves to the α3N site in a manner dictated by their relative affinities for Zn(II) at equilibrium. Once this occurs, metal bound at α3N may also preclude stable reassociation of the SmtB−DNA complex, thus making α3N a regulatory site as well. Once the intracellular free Zn(II) concentration has returned to unstressed levels, this Zn(II) must be removed for SmtB to regain its repressor function. It is tempting to speculate that this removal is carried out by partially metallated SmtA or apo-SmtA itself (*4*), through thiol ligand exchange reactions, much like eukaryotic metallothioneins that have been observed to transfer Zn(II) to and from Zn(II)-binding proteins (*23*, *24*). Experiments are underway to test this model.

Implications for Metal Selectivity of ArsR/SmtB Family Members. The observation that the α5 metal binding site is the regulatory Zn(II)-sensing site in SmtB leads to some interesting questions about the mode of regulation of other members of the ArsR/SmtB family of metalloregulatory metal sensor proteins. First, the α5 site is strictly conserved in members of the family known to sense Zn(II) (SmtB, ZiaR, and CzrA), in a manner that does not strictly require an intact α3N site (*17*). Second, a cysteine thiolate-rich α3 or α3N site is strictly conserved among members that sense larger, softer metals such as Cd(II), Pb(II), and Bi(III) (*10*−

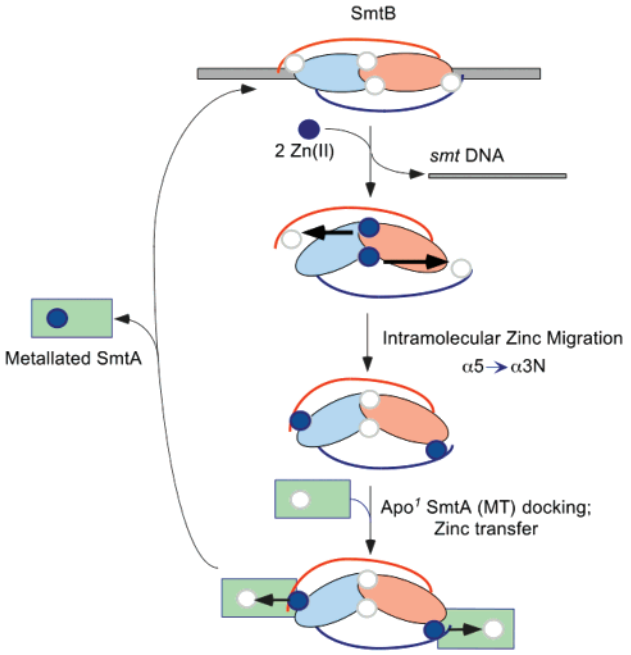

FIGURE 10: Hypothetical model of the DNA binding activity of SmtB in the presence of Zn(II). In this model, Zn(II) binds at the α5 site which induces dissociation of dimeric SmtB from the DNA (only a dimer is drawn for clarity, and the metal sites are assumed to be identical). This dissociation is followed by movement of the metal from the α5 site to the α3N site as dictated by their equilibrium affinities for Zn(II) (*17*); this in turn might facilitate intermolecular transfer of Zn(II) from SmtB to an acceptor protein, shown here as apo-SmtA or partially metalated (*4*) SmtA (see the text for details).

12, *25*). Work performed with *S. aureus* pI258 CadC reveals that two of four cysteine residues that comprise the α3N site (Cys7 and Cys60) are required for Cd(II) sensing in vitro (*25*) and in vivo (*12*) by CadC, with Cys60 being absolutely essential. Indeed, a C60G mutation in CadC is functionally inactive in vitro (*11*, *25*) and in vivo (*12*) despite forming stable nonnative coordination complexes with metal ions (*25*); this is a naturally occurring sequence variant in SmtB (Gly63), further support for the idea that Zn(II) sensing by SmtB and Cd(II) sensing by CadCs occur via two distinct allosteric pathways. Although most CadCs possess structurally intact α5 sites as predicted by the sequence alignment (*11*), we have argued that these sites may be vestigial in the evolution of a sensor domain designed to sense larger, more thiophilic metals, e.g., Cd(II) and Pb(II), which evolved on the periphery of the dimer (*11*). Along the same line of reasoning, the S_2NO α3N site in SmtB might simply endow SmtB with the ability to efficiently sense and detoxify a wider range of metals beyond simply Zn(II), e.g., Cd(II). In any case, our findings argue strongly that these two sites sense distinct metal ions and may play a primary role in dictating the metal specificities throughout the ArsR/SmtB family in vivo. Further studies on additional members of the family will lead to additional insight into the metalloregulatory mechanisms of these metal sensor systems.

ACKNOWLEDGMENT

We thank Dr. Nigel Robinson, University of Newcastle (Newcastle, U.K.), for many stimulating discussions.

REFERENCES

1. Robinson, N. J., Bird, A. J., and Turner, J. S. (1998) in *Metal ion in gene regulation* (Silver, S., and Walden, W., Eds.) pp 372−397, Chapman and Hall, New York.
2. Wu, J., and Rosen, B. P. (1993) *J. Biol. Chem. 268*, 52−58.
3. Cook, W. J., Kar, S. R., Taylor, K. B., and Hall, L. M. (1998) *J. Mol. Biol. 275*, 337−346.
4. Blindauer, C. A., Harrison, M. D., Parkinson, J. A., Robinson, A. K., Cavet, J. S., Robinson, N. J., and Sadler, P. J. (2001) *Proc. Natl. Acad. Sci. U.S.A. 98*, 9593−9598.
5. Morby, A. P., Turner, J. S., Huckle, J. W., and Robinson, N. J. (1993) *Nucleic Acids Res. 21*, 921−925.
6. VanZile, M. L., Cosper, N. J., Scott, R. A., and Giedroc, D. P. (2000) *Biochemistry 39*, 11818−11829.
7. O'Halloran, T. V. (1989) in *Metal ions in biological systems. Vol. 25. Interrelations among metal ions, enzymes, and gene expression* (Sigel, H., and Sigel, A., Eds.) pp 105−146, Marcel Dekker, New York and Basel.
8. Erbe, J. L., Taylor, K. B., and Hall, L. M. (1995) *Nucleic Acids Res. 23*, 2472−2478.
9. Kar, S. R., Lebowitz, J., Blume, S., Taylor, K. B., and Hall, L. M. (2001) *Biochemistry 40*, 13378−13389.
10. Busenlehner, L. S., Cosper, N. J., Scott, R. A., Rosen, B. P., Wong, M. D., and Giedroc, D. P. (2001) *Biochemistry 40*, 4426−4436.
11. Busenlehner, L. S., Apuy, J. L., and Giedroc, D. P. (2002) *J. Biol. Inorg. Chem. 7*, 551−559.
12. Sun, Y., Wong, M. D., and Rosen, B. P. (2001) *J. Biol. Chem. 276*, 14955−14960.
13. Turner, J. S., Glands, P. D., Samson, A. C. R., and Robinson, N. J. (1996) *Nucleic Acids Res. 19*, 3714−3721.
14. Thelwell, C., Robinson, N. J., and Turner-Cavet, J. S. (1998) *Proc. Natl. Acad. Sci. U.S.A. 95*, 10728−10733.
15. Singh, V. K., Xiong, A., Usgaard, T. R., Chakrabarti, S., Deora, R., Misra, T. K., and Jayaswal, R. K. (1999) *Mol. Microbiol. 33*, 200−207.
16. Kuroda, M., Hayashi, H., and Ohta, T. (1999) *Microbiol. Immunol. 43*, 115−125.
17. VanZile, M. L., Chen, X., and Giedroc, D. P. (2002) *Biochemistry 41*, 9765−9775.
18. Kar, S. R., Adams, A. C., Lebowitz, J., Taylor, K. B., and Hall, L. M. (1997) *Biochemistry 36*, 15343−15348.
19. Guo, J., and Giedroc, D. P. (1997) *Biochemistry 36*, 730−742.
20. Giedroc, D. P., Khan, R., and Barnhart, K. (1991) *Biochemistry 30*, 8230−8242.
21. Kuzmic, P. (1996) *Anal. Biochem. 237*, 260−273.
22. Endo, G., and Silver, S. (1995) *J. Bacteriol. 177*, 4437−4441.
23. Jacob, C., Maret, W., and Vallee, B. L. (1998) *Proc. Natl. Acad. Sci. U.S.A. 95*, 3489−3494.
24. Jiang, L.-J., Maret, W., and Vallee, B. L. (1998) *Proc. Natl. Acad. Sci. U.S.A. 95*, 3483−3488.
25. Busenlehner, L. S., Weng, T.-S., Penner-Hahn, J. E., and Giedroc, D. P. (2002) *J. Mol. Biol. 319*, 685−701.

BI020178T